

First-principles calculation of the thermodynamics of $\text{In}_x\text{Ga}_{1-x}\text{N}$ alloys: Lattice vibrations effects

Chee Kwan Gan¹, Yuan Ping Feng², and David J. Srolovitz³

¹*Institute of High Performance Computing, 1 Science Park Road, Singapore 117528, Singapore*

²*Department of Physics, National University of Singapore, 2 Science Drive 3, Singapore 117542, Singapore*

³*Department of Mechanical and Aerospace Engineering, Princeton University, Princeton, New Jersey, 08544*

The thermodynamics properties of the wurtzite and zinc-blende $\text{In}_x\text{Ga}_{1-x}\text{N}$ alloys are calculated using first-principles density-functional calculations. Special quasi-random structures are used to describe the disordered alloys, for $x = 1/4, 1/2$, and $3/4$. The effect of lattice vibrations on the phase diagram, commonly omitted from semiconductor alloy phase diagram calculations, are included through first-principles calculations of phonon spectra. Inclusion of lattice vibrations leads to a large reduction in the order-disorder critical temperature ($\sim 29\%$ and $\sim 26\%$ for the wurtzite and zinc-blende structures, respectively) and changes the shape of the solubility and spinodal curve through changes in the entropies of the competing phases. Neglect of such effect produces significant errors in the phase diagrams of complex ordered semiconductor compounds. The critical temperature for phase separation is 1654 K (1771 K) for the wurtzite (zinc-blende) structures. The predicted phase diagrams are in agreement with experimental measurements on MOCVD $\text{In}_x\text{Ga}_{1-x}\text{N}$ films.

PACS numbers: 71.22.+i, 64.75.+g, 63.50.+x

Keywords: phase diagrams, phase separation, lattice vibrations, compound semiconductors, InGa

I. INTRODUCTION

The group-III nitrides GaN and InN and their alloys have been receiving considerable attention for high-power, high-frequency, and high-temperature optoelectronic applications, such as light emitting and laser diodes. By changing composition one can, in principle, continuously tune the band gap from 0.8 eV (InN)¹ to 3.5 eV (GaN) — a range that spans much of the visible spectrum. However, because of the large lattice mismatch between GaN and InN ($\sim 11\%$ for the a and c -directions in the wurtzite structure), the solid solution has a tendency to undergo phase separation.^{2,3,4} GaN, InN and their alloys ($\text{In}_x\text{Ga}_{1-x}\text{N}$), grown under ambient conditions, typically assume the hexagonal wurtzite (WZ) crystal structure.^{3,4,5,6} It is possible, however, to grow thin epitaxial films of $\text{In}_x\text{Ga}_{1-x}\text{N}$ with the cubic zinc-blende (ZB) structure.^{7,8,9,10,11,12,13,14} The phase stability of $\text{In}_x\text{Ga}_{1-x}\text{N}$ alloys has been the subject of several experimental^{3,4} and theoretical studies^{15,16,17,18,19,20,21,22,23,24}. For example, there have been more than ten calculations of the $\text{In}_x\text{Ga}_{1-x}\text{N}$ pseudo-binary phase diagram. These have included valence-force field (VFF)^{15,16,17}, tight-binding, and density functional calculations¹⁸, sometimes combined with atomic-scale Monte Carlo simulations¹⁹. Surprisingly, there is considerable discrepancy in the predicted miscibility gap. The tendency for phase separation is largely driven by the relatively large misfit strains²². The predicted critical temperature varies over a 2000 K range, with most calculations predicting $1500 \text{ K} \leq T_c \leq 2000 \text{ K}$. The source of this discrepancy may be associated with the accuracy of the description of the atomic interactions, the need for a statistically meaningful description of the distribution of Ga and In on the solid so-

lution cation sites and the contribution to the free energy associated with configurational entropy²⁰. Additionally, the vibrational contribution to the free energy has never been included. In the present paper, we report the results of the most rigorous calculation of this phase diagram performed to date. The results clearly demonstrate the importance of the vibrational contribution in determining phase diagrams in semiconductor alloys, such as $\text{In}_x\text{Ga}_{1-x}\text{N}$.

In this work, we employ accurate density-functional theory (DFT) to examine the thermodynamic properties of both wurtzite and zinc-blende $\text{In}_x\text{Ga}_{1-x}\text{N}$. We directly compare the formation enthalpy and free energy differences determined using exactly the same pseudopotentials and energy cutoff for both structures. Using these results, we predict the binodal and spinodal on the binary phase diagram; delineating the miscibility gap and the region where the solid solution is unstable. The simulation method uses the special quasirandom structure (SQS) formalism^{25,26} to faithfully (and efficiently) represent the structure of the random alloy. The effect of lattice vibrations, often neglected in semiconductor alloy thermodynamic calculations, is included in a harmonic approximation where the dynamical matrix is determined using density-functional theory methods. Even though lattice vibration effects have been shown to be significant for the thermodynamic properties of some intermetallics²⁷, the effects of vibration have been commonly neglected for semiconductor alloys. Such effects were not previously included, in part, because an accurate treatment of lattice vibrations requires substantial computing resources, above that needed for modeling the effects of alloying on the heat of formation. Advances in first-principles computational methods and hardware make routine inclusion of vibrational effects in alloy phase di-

agram calculations possible. As we demonstrate below, lattice vibrations can drastically alter calculated thermodynamic properties and phase diagrams of $\text{In}_x\text{Ga}_{1-x}\text{N}$. This work provides the first direct evaluation of the significance of lattice vibration effects on the phase diagram of compound semiconductor alloys — a large and technologically important class of complex alloys. Earlier work on solid solution semiconductor alloys Si-Ge²⁸ and $\text{Ga}_{1-x}\text{In}_x\text{P}$ ²⁹ suggested that lattice vibration effects are negligible. On the other hand, inclusion of these effects on metallic compounds (intermetallics) have been shown to be important in determining phase stability in the Cd-Mg³⁰, Al-Sc³¹, Cu-Au³², and Al-Cu³³ systems. However, vibration effects have been shown to be relatively unimportant in other metallic systems that exhibit compound formation, e.g., Ni-Al³⁴ and Pd-V³⁵. The previous work on the phase stability of metals suggests that vibrational effects may or may not be important in those systems. Further, there is no evidence to support the idea that one can extrapolate from metals to compound semiconductor alloys.

The solid state $\text{In}_x\text{Ga}_{1-x}\text{N}$ phase diagrams, determined herein, represent the most rigorous determinations reported to-date. The resultant phase diagram shows that the wurtzite crystal structure is more stable than the zinc-blende structure over the entire $\text{In}_x\text{Ga}_{1-x}\text{N}$ composition and temperature ranges examined.

II. PREVIOUS THEORETICAL CALCULATIONS

Due to its low computation cost and relative accuracy, valence-force-field (VFF) models³⁶ have been used extensively to study^{15,16,17,19} the $\text{In}_x\text{Ga}_{1-x}\text{N}$ alloy system. One of the first $\text{In}_x\text{Ga}_{1-x}\text{N}$ phase diagram calculations was performed by Ho and Stringfellow¹⁵, who employed a VFF model to investigate the solid phase miscibility gap in zinc-blende $\text{In}_x\text{Ga}_{1-x}\text{N}$. They found a critical temperature of 1523 K and that at the growth temperature of 800°C, the InN solubility in GaN is less than 6%. Using interaction constants deduced from first-principles calculations, Saito and Arakawa¹⁶ simulated the wurtzite $\text{In}_x\text{Ga}_{1-x}\text{N}$ alloy system using the VFF model and obtained a critical temperature of 1690 K. Takayama *et al.*¹⁷, using a modified VFF for $\text{In}_x\text{Ga}_{1-x}\text{N}$, found a critical temperature of 1668 K for the zinc-blende structure and 1967 K for the wurtzite structure.

Several first-principles calculations have also been performed. Van Schilfgaarde *et al.*¹⁸ relaxed a 32-atom structure using a tight-binding method and determined the heat of formation using density-functional theory. Combining this result with an ideal mixing estimate of the configurational entropy led to critical temperatures of 3980 K and 2290 K for the wurtzite and zinc-blende structures, respectively. These values are considerably higher than those obtained from the VFF models. Teles *et al.*²² investigated strained and relaxed $\text{In}_x\text{Ga}_{1-x}\text{N}$ al-

loys using a pseudopotential plane-wave approach with a generalized quasichemical approximation (GQCA) for mixing³⁷. They obtained a critical temperature of 1295 K for the zinc-blende $\text{In}_x\text{Ga}_{1-x}\text{N}$, which is lower than the VFF results^{15,17}. Another first-principles calculation²³ also reported a similar value for the critical temperature (i.e., 1400 K) for zinc-blende $\text{In}_x\text{Ga}_{1-x}\text{N}$.

Grosse and Neugebauer³⁸ assessed the limits and accuracy of the VFF models for $\text{In}_x\text{Ga}_{1-x}\text{N}$ alloys by studying various ordered structures using first-principles calculations. They found that while VFF works reasonably well for some zinc-blende III/V semiconductors, significant errors occur for group III nitrides (GaN, InN). In particular, the formation energies for alloys are significantly underestimated (by 14 meV/cation). These findings suggest that the critical temperature of $\text{In}_x\text{Ga}_{1-x}\text{N}$ obtained from first-principles calculations should be higher than those from VFF calculations. However, this conclusion is inconsistent with the predictions of VFF^{15,16,17} and first-principles results^{22,23} (i.e., the T_c values from VFF studies exceed those from first-principles calculations). Our results, presented below, shed light on this discrepancy.

III. SPECIAL QUASIRANDOM STRUCTURES

The effects of disorder on the stability and structure of alloys have received considerable attention over the past few decades. The coherent-potential approximation (CPA)³⁹ for describing such effects is a single-site theory that treats the random A_xB_{1-x} alloys by considering the average occupations of lattice sites by atoms A and B. Hence the effects of local environment such as charge transfer, local chemical environment, and local structural relaxation are ignored. However, local environment effects have been shown to be important in determining the thermodynamics and electronic properties of alloys^{25,26}. One approach to incorporate the local environment effect is through first-principles density-functional theory. One can, in principle, model a disordered A_xB_{1-x} system using a plane-wave density-functional methods with a large supercell in which A and B are distributed at random on lattice sites. Unfortunately, since computational costs in such methods usually scale with the number of atoms in the supercell, N as N^3 , one is usually forced to use a small supercell. Small supercells invariably lead to poor statistics and spurious correlations (i.e., this approach leads to a chemical environment about each site which is different from that in a large, truly random system). Zunger *et al.*^{25,26} recognized that most physical properties are governed by atomic interactions between near neighbors and developed a method to generate atomic arrangements in small supercells that correctly reproduce the short and intermediate range correlations that exist in random alloys. These structures are called special-quasirandom-structures (SQS).

A useful approach to defining correlation functions in

crystals with different site occupancies is to assign each site i a variable according to the type of occupying atom, say $s_i = +1$ for an A atom and $s_i = -1$ for an B atom. Next, we make a list of pairs of atoms in our structure that are separated by k or less nearest neighbor distances and evaluate the product $\pi = s_i s_j$ for that particular pair of atoms on sites i and j . Averaging this value over all such pairs in the structure yields the correlation function $\Pi_{2,k}$, where the two indicates we are considering pairs. We can use a similar procedure for triplets, quadruplets,.. m -lets of atoms to produce a series of correlation functions $\Pi_{m,k}$. If the alloy were of infinite extent and the site occupancies were truly random, all $\Pi_{m,k}$ would be $\Pi_{m,k}(x) = \bar{\Pi}_m(x) = [(+1)x + (-1)(1-x)]^m = (2x-1)^m$, where x is the concentration of A atoms in the system.

We have implemented the SQS algorithm for different unit cell sizes and shapes, generating all possible site occupancies for the chosen x , calculating $\Pi_{m,k}$ and keeping the configuration for which the set of $\Pi_{m,k}(x)$ is closest to $\bar{\Pi}_m(x)$. In practice, we use only $m = 2$ and $k \leq 10$. We repeat this procedure for different unit cell shapes, as described by the supercell lattice vectors \mathbf{a}_1 , \mathbf{a}_2 , and \mathbf{a}_3 , and retain the one that leads to the best correlation with random occupancy (using our implementation of the procedure described in Refs. 40,41).

In this work we have focused on wurtzite and zinc-blende crystal structures with 16 cations and 16 anions per unit cell. The occupancies, in our case correspond to Ga or In on the cation sites. The descriptions of the hexagonal-close-packed (hcp) and face-centered-cubic (fcc) sublattices are shown in Tables I and II, respectively. For $x = 1/4$ (or $x = 3/4$), the wurtzite structure delivers exact matches up to $\Pi_{2,5}$ and up to $\Pi_{2,7}$ for $x = 1/2$. For the zinc-blende structure, we find structures that yield correlation functions that exactly match the random case up to $\Pi_{2,3}$ for $x = 1/4$ (or $x = 3/4$) and to $\Pi_{2,7}$ for $x = 1/2$. Unlike in previous studies of $\text{In}_x\text{Ga}_{1-x}\text{N}$ alloys²³, the present analysis provides a quantitative measure of the degree to which the simulation cell resembles a random alloy. Based on the quoted pair statistics, we conclude that the unit cells and occupancies employed herein provide good representations of the set of wurtzite and zinc-blende random alloys.

IV. FORMATION ENTHALPY CALCULATIONS

We first optimize the zinc-blende (wurtzite) GaN and InN structures with respect to the atomic coordinates and the unit cell parameter(s) a (and c) using the first-principles density-functional^{42,43} method within the local density approximation (LDA). This was done using the plane-wave pseudopotential Vienna *ab initio* simulation package (VASP)⁴⁴ non-norm-conserving pseudopotentials.⁴⁵ The important^{38,46} 3d states for Ga and 4d states for In are included as valence electrons in the pseudopotentials. A relatively high cutoff energy of 31.96 Ry is used throughout this work. A Monkhost-

Pack mesh of $7 \times 7 \times 7$ is used for the 4-atom unit cell wurtzite InN and GaN systems. A $5 \times 5 \times 5$ mesh is used for the 8-atom zinc-blende InN and GaN unit cells (finer meshes resulted in total energy changes of less than 0.1 meV/atom). Table III shows that the relaxed lattice parameters for GaN and InN in both the wurtzite and zinc-blende structures are in good agreement with other theoretical and experimental work. The wurtzite GaN (InN) structures have lower total energies than zinc-blende GaN (InN) by 13 meV/cation (18 meV/cation). This is in good agreement with the calculations of Groose and Neugebauer, where the wurtzite GaN (InN) is lower in total energy than the zinc-blende GaN (InN) by 11 meV/cation (19 meV/cation).

We determine the equilibrium structure by minimizing the total energy of the system with respect to the lattice parameters and the positions of each of the 32 ions within the SQS cell. The formation enthalpy of the alloy is

$$\Delta H_Y = E_Y(\text{In}_x\text{Ga}_{1-x}\text{N}) - xE_{\text{WZ}}(\text{InN}) - (1-x)E_{\text{WZ}}(\text{GaN}), \quad (1)$$

where $x = 0, 1/4, 1/2, 3/4$, or 1, and where Y represents either wurtzite (WZ) or zinc-blende (ZB). The wurtzite crystals are used as references for both the wurtzite and zinc-blende cases, such that the two can be easily compared. The formation enthalpy results are shown in Fig. 1. We fit this data to the form¹⁶ $\Delta H = (\alpha + \beta x)x(1-x)$ (i.e., beyond regular solution theory). For the wurtzite structure, we obtain $\alpha = 0.4050$ eV/cation and $\beta = -0.1117$ eV/cation. For zinc-blende, we find $\alpha = 0.4223$ eV/cation and $\beta = -0.1088$ eV/cation.

Consistent with the results of Saito and Arakawa¹⁶ (see Fig. 1), we find that all of the curves are skewed slightly to the left. Focusing on the wurtzite results, we see that the valence force field (VFF) predictions for the heat of formation¹⁶ are significantly smaller than those obtained here (by as much as 15.4 meV/cation at $x = 1/2$). That the heat of formation obtained from the the VFF is smaller than the first principles predictions was first noted by Grosse and Neugebauer³⁸ (by 14.2 meV/cation in their case).

V. PHONON CALCULATIONS

The phonon contribution to the free energy was determined within the harmonic approximation using the supercell force-constant method^{47,48,49,50} to calculate the phonon density of states. In this approach, each atom is displaced and the forces acting on each of the other (static) atoms are calculated and used to determine the matrix of force constants. We then calculate the dynamical matrix for several reciprocal lattice vectors \mathbf{q} and diagonalized these to find the phonon eigen-frequencies ω and vectors. Integrating the phonon eigen-frequencies over the Brillouin zone yields the phonon density of states $g(\omega)$. At atmospheric pressure, the difference between the Gibbs and Helmholtz free energies is negligible for

the condensed phase. Therefore, we calculate the phonon free energy G_v for an N -atom supercell as a function of temperature T as

$$G_v(T) = Nk_B T \int_0^\infty d\omega g(\omega) \log \left[2 \sinh \left(\frac{\hbar\omega}{2k_B T} \right) \right], \quad (2)$$

where $g(\omega)$ is normalized according to $\int_0^\infty d\omega g(\omega) = 3$.

The displacements of the atoms used to calculate the force constants must be small enough such that the system behaves harmonically yet large enough that the forces are sufficiently large as to be reliable. In our implementation of the vibrational thermodynamics code, we employ a displacement of 0.03 \AA^{51} . Because of the low symmetry inherent to the random solid solution, each atom in the SQS unit cell is displaced individually. For the wurtzite structure, we use a supercell of 64 atoms (twice as large as the 16 cation SQS) to reduce the effect of periodic images for the determination of force constants. For GaN and InN in the wurtzite structure, we use a supercell consists of $3 \times 3 \times 3$ four-atom wurtzite primitive cell. For the zinc-blende structure, we use 64-atom supercells for all x . The LO/TO splitting, associated with long range dipole-dipole interactions affects a small region near the center of the Brillouin zone, was not considered here (for computational efficiency). This should introduce only very small errors in the free energy of formation of the alloy⁵². It is possible to account for the LO/TO splitting using density functional perturbation theory (DFPT)^{53,54}.

The calculated phonon densities of states of both wurtzite and zinc-blende $\text{In}_x\text{Ga}_{1-x}\text{N}$ are shown in Fig. 2 for several alloy compositions. The density of states shifts to lower frequencies as the indium concentration is increased, as expected since (1) In atoms have a larger mass than Ga atoms and (2) InN has a lower⁴⁶ bulk modulus (1.39 Mbar) than GaN (2.02 Mbar). These two effects are of the same magnitude and together explain most of the shift in the vibrational frequencies in going from GaN to InN. Alloying InN with Ga (or vice versa) decreases the magnitudes of the peaks in the DOS while broadens the frequency range. The broadening of the phonon spectra on alloying is associated with disorder reducing the coherence of the phonon modes.

We calculate the vibrational free energy difference $\Delta G_{v,Y}$ (Y is ZB or WZ) as

$$\Delta G_{v,Y} = G_{v,Y}(\text{In}_x\text{Ga}_{1-x}\text{N}) - xG_{v,WZ}(\text{InN}) - (1-x)G_{v,WZ}(\text{GaN}), \quad (3)$$

where the same wurtzite reference frame is used. Figure 3 shows that $\Delta G_{v,Y}$ is a nearly linear function of temperature for all compositions. For (nearly) all compositions, $\Delta G_{v,Y}(x)$ for the wurtzite structure lies below those for the zinc-blende. The vibrational contribution to the entropy of formation ($\Delta S_v = -\partial\Delta G_v/\partial T$) is larger for the alloys ($0 < x < 1$) than for $x = 0$ or 1 (the negative $\Delta S_{v,ZB}$ at some compositions is an artifact of using wurtzite as the reference structure). We note that ΔG_v for wurtzite $\text{In}_{1/4}\text{Ga}_{3/4}\text{N}$ is lower

than that for $\text{In}_{1/2}\text{Ga}_{1/2}\text{N}$. However, the ΔG_v for zinc-blende $\text{In}_{1/4}\text{Ga}_{3/4}\text{N}$ is higher than that for zinc-blende $\text{In}_{1/2}\text{Ga}_{1/2}\text{N}$. We can fit $\Delta G_{v,Y}(x)$ to the same type of interpolation function as used for the enthalpy of formation, where the parameters α and β in the fit are functions of temperature.

According to Eq. 3, $\Delta G_v(x)$ is the difference in the vibrational contribution to the free energy between the solid solution alloy and the terminal compounds. This difference can be traced to the difference in phonon density of states (Fig. 2 and Eq. 2) between the alloy $g_{\text{In}_x\text{Ga}_{1-x}\text{N}}(\omega)$ and the composition weighted average of the density of states of GaN and InN; i.e., $g_{\text{av}}(\omega) = xg_{\text{InN}}(\omega) + (1-x)g_{\text{GaN}}(\omega)$. Comparing $g_{\text{In}_x\text{Ga}_{1-x}\text{N}}(\omega)$ and $g_{\text{av}}(\omega)$ in Fig. 2, we see that $g_{\text{av}}(\omega)$ is on balance shifted to larger ω at each x (except $x = 0$ or 1, of course). The density of states at large frequencies ω makes a larger (more positive) contribution to the vibrational free energy than do those at small frequencies. This explains why lattice vibrations lead to negative values of ΔG_v . We return to this point below.

VI. PSEUDO-BINARY PHASE DIAGRAM

The free energy of formation ΔG of the $\text{In}_x\text{Ga}_{1-x}\text{N}$ is given by

$$\Delta G = \Delta H - T\Delta S + \Delta G_v. \quad (4)$$

As described above, ΔH and ΔG_v in this equation are known from fitting the DFT and phonon calculations to particular functional forms. ΔS corresponds to the entropy of mixing and, in the present analysis, is described in the Bragg-Williams approximation as $\Delta S = -k_B[x \log x + (1-x) \log(1-x)]$ (per cation). As is well-known, the Bragg-Williams approximation can be severe. However, the resulting errors are important, predominantly in frustrated systems and systems where the phase diagram has a complex topology⁵⁵. Neither of these situations apply to the $\text{In}_x\text{Ga}_{1-x}\text{N}$ system. The Bragg-Williams approximation was also applied in many of the earlier calculations of the $\text{In}_x\text{Ga}_{1-x}\text{N}$ phase diagram discussed above^{15,16,17,18}.

We employ the same wurtzite reference state for the unmixed GaN and InN in order to make a meaningful comparison of the free energies of $\text{In}_x\text{Ga}_{1-x}\text{N}$. Figure 4 shows ΔG for both the wurtzite and zinc-blende structures. The wurtzite structure has a lower free energy than the zinc-blende structure at $T = 1000 \text{ K}$ by approximately 0.15 eV/cation. Further numerical investigation reveals that wurtzite structure has a smaller free energy than the zinc-blende structure at all temperatures and composition x investigated. This suggests that the wurtzite structure is always more stable than the zinc-blende structure in this alloy system, in agreement with experimental observations.

The equilibrium solubility limits (the binodal curve) as a function of temperature are calculated using a com-

mon tangent approach⁵⁶, as shown in Fig. 4 for 1000 K. Figure 5 shows that the critical temperature below which phase separation will occur at some composition, T_c , is 2132 K for the wurtzite structure in the absence of vibrational contributions to the free energy. Zinc-blende $\text{In}_x\text{Ga}_{1-x}\text{N}$ shows $T_c = 2231$ K when vibrational effects are excluded. These values of T_c (for both the wurtzite and zinc-blende structures) are higher than other VFF results^{15,16,17} that neglect vibrations. These differences are attributable to the fact that the formation enthalpy determined from our DFT calculations are larger than those obtained within the VFF (e.g., see Fig. 1). Our predicted $T_c = 2231$ K (for zinc-blende structure without vibrations) is considerably higher than those obtained by Teles *et al.*²² ($T_c = 1295$ K). This is probably attributable to the relatively small (8-atom) supercells that they employed. We note that another DFT calculation²³, with larger clusters (64 atoms/cell), predicts a slightly higher $T_c = 1400$ K. The discrepancy that still remains is likely the result of the better description of the random solid solution alloy used in our analysis.

Inclusion of the lattice vibrational effect reduces (see Fig. 5) T_c for the wurtzite $\text{In}_x\text{Ga}_{1-x}\text{N}$ from 2132 K to 1654 K, a decrease of 29%. For zinc-blende structure, T_c is reduced from 2231 K to 1771 K. The change in the critical temperature upon inclusion of the vibrational contributions suggests that omission of this term may be one of the most significant errors commonly made in the calculation of phase diagrams of compound semiconductor alloys. Since this contribution is largely entropic and is larger in the disordered phase, it will generally lead to a decrease in the stability of the ordered phase relative to the disordered phase and, therefore, to a lower T_c . The origin of this effect can be traced to the broadening of the vibrational density of state with increasing disorder, as shown in Fig. 2. Inclusion of the vibrational contribution to the free energy also makes the wurtzite $\text{In}_x\text{Ga}_{1-x}\text{N}$ phase diagram more symmetric with a peak at $x = 0.47$ with vibrations, as compared to $x = 0.39$ without. The maximum in the binodal in the zinc-blende diagram also shifts closer to $x = 0.5$ with inclusion of vibrational effects (although in this case the effect is weaker than in the wurtzite case). We also note that inclusion of vibrations does not significantly increase the solubilities of In in GaN or Ga in InN, except above approximately 1200 K.

Another effect of vibrations is to decrease the width of the 2-phase field in the phase diagram at all temperatures (relative to the phase diagram that does not include the vibration effect). A common goal in the growth of $\text{In}_x\text{Ga}_{1-x}\text{N}$ alloys for microelectronic applications is to increase the range of compositions that are achievable without phase separation (i.e., increase the solubility limits). Examination of the phase diagram in Fig. 5 shows that this could be accomplished simply by increasing the growth temperature. This is not always possible. An alternative approach is to increase the entropy of the disordered alloy relative to that of the phase separated

material. This could be accomplished through alloying (quaternary additions). Addition of a new component increases the configurational entropy of the alloy. The present results suggests that alloying could also be used to increase the vibrational contribution to the stability of the disordered phase. This would be most effective with the addition of heavier elements, which shift the vibrational frequencies to lower values and therefore increase the width of the vibrational density of state (see Fig. 2). Of course, the new alloy component should not increase the enthalpy of formation of the disordered phase.

Figure 6 shows a comparison of the wurtzite and zinc-blende $\text{In}_x\text{Ga}_{1-x}\text{N}$ phase diagrams (including the effects of lattice vibrations). The wurtzite structure has a lower T_c and is more symmetric (with respect to composition) than is the zinc-blende structure. These differences can be important in cases where the zinc-blende structure is stabilized through heteroepitaxy^{12,14} or other means.

A direct comparison of the predicted phase diagram with an experimental phase diagram cannot be made since the latter has never been determined. However, an experimental study⁴ of $\text{In}_{0.09}\text{Ga}_{0.91}\text{N}$ showed that this alloy does not phase separate at the growth temperature of 923 K. According to the phase diagram in Fig. 6, this composition and temperature lies between the binodal and spinodal. This suggests that the solid solution is metastable, with respect to phase separation. Additional experimental measurements⁴ show that phase separation occurs in samples grown at both $\text{In}_{0.37}\text{Ga}_{0.63}\text{N}$ and $\text{In}_{0.35}\text{Ga}_{0.65}\text{N}$ and 998 K. This is also consistent with the predicted phase diagram — these growth conditions are within the spinodal region, where the disordered alloy is unstable. Since these materials were produced by MOCVD, there is some uncertainty as to whether the phases observed correspond to the bulk equilibrium phases at this temperature. In such cases, the phases that are observed may be influenced/inherited from the surface structure and by hetero-epitaxial strains. However, a solid solution cannot be stable within the spinodal region of the phase diagram, independent of how the material was produced (slow diffusional kinetics may limit the rate at which such an instability grows).

The phase diagrams presented here constructed based upon several assumptions. These include a harmonic description of the phonons in a relatively small unit cell, a Bragg-Williams approximation for the entropy of mixing and that the solid solution has no short-range order. All approximations employed in this work can be improved by using larger unit cells, a quasi-harmonic model for the vibrational contributions to the free energy, more accurate treatment of the entropy of mixing (e.g., using a cluster variational approach⁵⁷) and a self-consistent determination of the short-range order. Despite the nature of the approximations made, the predicted results represent the most rigorous determination of the $\text{In}_x\text{Ga}_{1-x}\text{N}$ phase diagram to date.

VII. SUMMARY

We have employed accurate density-functional calculations to study the thermodynamic properties of both the zinc-blende and wurtzite structures of $\text{In}_x\text{Ga}_{1-x}\text{N}$. The disordered alloy was modeled using the quasi-random structure (SQS) approach to ensure that the order parameter accurately describes a random solid solution (the detailed SQS structure information is provided for the 16-cation unit cells for both the zinc-blende and wurtzite structures). The vibrational contribution to the free energy has been calculated using first-principles calculations of the phonon spectra within the harmonic approximation. Inclusion of these effects leads to a 29% (26%) reduction in the critical temperature for phase separation in the wurtzite (zinc-blende) structure. We found that the wurtzite structure is thermodynamically more stable than zinc-blende structure at all temperatures and alloy compositions. The predicted miscibility gap and spinodal curve are consistent with experimental observations on MOCVD $\text{In}_x\text{Ga}_{1-x}\text{N}$. Nonetheless, care must be exercised in interpreting the phases observed following such growth processes in terms of an equilibrium phase diagram.

The present results suggest that inclusion of the vibrational contribution to the free energy of formation of compound semiconductor alloys can have a profound effect on

the critical temperature for the order-disorder transition on the cation sublattice. This issue is particularly important for the increasingly complex compound semiconductors of interest today. Not only does the vibrational entropy shift the critical temperature, it also modifies the solubility limits of each component and does so in a non-symmetric manner. The present results also point to the importance of determining all of the contributions to the free energy self-consistently; that is using the same energetics description for relaxing the atomic structures, calculating enthalpies of formation and vibrational contributions to the free energy. While the present results represents a significant advance in compound semiconductor alloy phase diagram calculations, further improvements should include the effects of short range order in the disordered phase and better approximations to the entropy of mixing (see e.g., Ref. 57).

VIII. ACKNOWLEDGMENTS

The authors gratefully acknowledge useful discussions with C. Jiang, A. van de Walle and D. Vanderbilt. This work was supported by Visiting Investigator Program, Agency for Science, Technology and Research (A*STAR), Singapore.

-
- ¹ Y. Nanishi, Y. Saito, and T. Yamaguchi, *Jpn. J. Appl. Phys.* **42**, 2549 (2003).
 - ² K. Osamura, S. Naka, and Y. Murakami, *J. Appl. Phys.* **46**, 3432 (1975).
 - ³ N. A. El-Masry, E. L. Piner, S. X. Liu, and S. M. Bedair, *Appl. Phys. Lett.* **72**, 40 (1998).
 - ⁴ D. Doppalapudi, S. B. Basu, J. K. F. Ludwig, and T. D. Moustakas, *J. Appl. Phys.* **84**, 1389 (1998).
 - ⁵ R. Singh, D. Doppalapudi, T. D. Moustakas, and L. T. Romano, *Appl. Phys. Lett.* **70**, 1089 (1997).
 - ⁶ Y. Sato and S. Sato, *Jpn. J. Appl. Phys.* **36**, 4295 (1997).
 - ⁷ M. J. Paisley, Z. Sitar, J. B. Posthill, and R. F. Davis, *J. Vac. Sci. Technol. A* **7**, 701 (1989).
 - ⁸ O. Brandt, H. Yang, B. Jenichen, Y. Suzuki, L. Daweritz, and K. H. Ploog, *Phys. Rev. B* **52**, R2253 (1995).
 - ⁹ D. Schikora, M. Hankeln, D. J. As, K. Lischka, T. Litz, A. Waag, T. Buhrow, and F. Henneberger, *Phys. Rev. B* **54**, R8381 (1996).
 - ¹⁰ H. Yang, L. X. Zheng, J. B. Li, X. J. Wang, D. P. Xu, Y. T. Wang, X. W. Hu, and D. D. Han, *Appl. Phys. Lett.* **74**, 2498 (1999).
 - ¹¹ H. Gamez-Cuatzin, J. Tardy, P. Rojo-Romeo, A. Philippe, C. Bru-Chevalier, A. Souifi, G. Guillot, E. Martinez-Guerrero, G. Feuillet, B. Baudin, et al., *Phys. Stat. Sol. (A)* **176**, 131 (1999).
 - ¹² Y. Taniyasu, K. Suzuki, D. H. Lim, A. W. Jia, M. Shimotomai, Y. Kato, M. Kobayashi, A. Yoshikawa, and K. Takahashi, *Phys. Stat. Sol. (A)* **180**, 241 (2000).
 - ¹³ H. Okumura, H. Hamaguchi, T. Koizumi, K. Balakrishnan, Y. Ishida, M. Arita, S. Chichibu, H. Nakanish, T. Natatomo, and S. Yoshida, *J. Cryst. Growth* **189/190**, 390 (1998).
 - ¹⁴ A. Tabata, J. R. Leite, A. P. Lima, E. Silveira, V. Lemos, T. Frey, D. J. As, D. Schikora, and K. Lischka, *Appl. Phys. Lett.* **75**, 1095 (1999).
 - ¹⁵ I. H. Ho and G. B. Stringfellow, *Appl. Phys. Lett.* **69**, 2701 (1996).
 - ¹⁶ T. Saito and Y. Arakawa, *Phys. Rev. B* **60**, 1701 (1999).
 - ¹⁷ T. Takayama, M. Yuri, K. Ito, T. Baba, and J. J. S. Harris, *J. Appl. Phys.* **88**, 1104 (2000).
 - ¹⁸ M. van Schilfgaarde, A. Sher, and A. B. Chen, *J. Cryst. Growth* **178**, 8 (1997).
 - ¹⁹ J. Adhikari and D. A. Kofke, *J. Appl. Phys.* **95**, 4500 (2004).
 - ²⁰ S. Y. Karpov, N. I. Podolskaya, I. A. Zhmakin, and A. I. Zhmakin, *Phys. Rev. B* **70**, 235203 (2004).
 - ²¹ T. Matsuoka, *Appl. Phys. Lett.* **71**, 105 (1997).
 - ²² L. K. Teles, J. Furthmüller, L. M. R. Scolfaro, J. R. Leite, and F. Bechstedt, *Phys. Rev. B* **62**, 2475 (2000).
 - ²³ M. Ferhat and F. Bechstedt, *Phys. Rev. B* **65**, 075213 (2002).
 - ²⁴ J. A. Purton, M. Y. Lavrentiev, and N. L. Allan, *J. Mater. Chem.* **15**, 785 (2005).
 - ²⁵ A. Zunger, S. H. Wei, L. G. Ferreira, and J. E. Bernard, *Phys. Rev. Lett.* **65**, 353 (1990).
 - ²⁶ S. H. Wei, L. G. Ferreira, J. E. Bernard, and A. Zunger, *Phys. Rev. B* **42**, 9622 (1990).
 - ²⁷ A. van de Walle and G. Ceder, *Rev. Mod. Phys.* **74**, 11 (2002).
 - ²⁸ G. D. Garbulsky, Ph.D. thesis, Massachusetts Institute of

- Technology, Cambridge, MA (1996).
- ²⁹ A. Silverman, A. Zunger, R. Kalish, and J. Adler, *J. Phys.: Condens. Matter* **7**, 1167 (1995).
 - ³⁰ M. Asta, R. McCormack, and D. de Fontaine, *Phys. Rev. B* **48**, 748 (1993).
 - ³¹ V. Ozoliņš and M. Asta, *Phys. Rev. Lett.* **86**, 448 (2001).
 - ³² V. Ozoliņš, C. Wolverton, and A. Zunger, *Phys. Rev. B* **58**, R5897 (1998).
 - ³³ C. Wolverton and V. Ozoliņš, *Phys. Rev. Lett.* **86**, 5518 (2001).
 - ³⁴ A. van de Walle, G. Ceder, and U. V. Waghmare, *Phys. Rev. Lett.* **80**, 4911 (1998).
 - ³⁵ A. van de Walle and G. Ceder, *Phys. Rev. B* **61**, 5972 (2000).
 - ³⁶ P. N. Keating, *Phys. Rev.* **145**, 637 (1966).
 - ³⁷ A. Sher, M. van Schilfgaarde, A. B. Chen, and W. Chen, *Phys. Rev. B* **36**, 4279 (1987).
 - ³⁸ F. Grosse and J. Neugebauer, *Phys. Rev. B* **63**, 085207 (2001).
 - ³⁹ H. Ehrenreich and L. M. Schwartz, in *Solid State Physics*, edited by H. Ehrenreich, F. Seitz, and D. Turnbull (Academic, New York, 1976), p. 149.
 - ⁴⁰ C. Jiang, C. Wolverton, J. Sofo, L. Q. Chen, and Z. K. Liu, *Phys. Rev. B* **69**, 214202 (2004).
 - ⁴¹ A. van de Walle, M. Asta, and G. Ceder, *CALPHAD: Comput. Coupling Phase Diagrams Thermochem.* **26**, 539 (2003).
 - ⁴² P. Hohenberg and W. Kohn, *Phys. Rev.* **136**, 864B (1964).
 - ⁴³ W. Kohn and L. J. Sham, *Phys. Rev.* **140**, 1133A (1965).
 - ⁴⁴ G. Kresse and J. Furthmüller, *Phys. Rev. B* **54**, 11169 (1996).
 - ⁴⁵ D. Vanderbilt, *Phys. Rev. B* **41**, R7892 (1990).
 - ⁴⁶ A. F. Wright and J. S. Nelson, *Phys. Rev. B* **51**, 7866 (1995).
 - ⁴⁷ W. Frank, C. Elsässer, and M. Fähnle, *Phys. Rev. Lett.* **74**, 1791 (1995).
 - ⁴⁸ G. Kresse, J. Furthmüller, and J. Hafner, *Europhys. Lett.* **32**, 729 (1995).
 - ⁴⁹ K. Parlinski, Z.-Q. Li, and Y. Kawazoe, *Phys. Rev. Lett.* **78**, 4063 (1997).
 - ⁵⁰ G. J. Ackland, M. C. Warren, and S. J. Clark, *J. Phys.: Condens. Matter* **9**, 7861 (1997).
 - ⁵¹ K. Parlinski and Y. Kawazoe, *Phys. Rev. B* **60**, 15511 (1999).
 - ⁵² A. van de Walle (2005), private communication.
 - ⁵³ P. Giannozzi, S. de Gironcoli, P. Pavone, and S. Baroni, *Phys. Rev. B* **43**, 7231 (1991).
 - ⁵⁴ S. Baroni, S. de Gironcoli, A. D. Corso, and P. Giannozzi, *Rev. Mod. Phys.* **73**, 515 (2001).
 - ⁵⁵ D. de Fontaine, *Solid State Phys.* **34**, 73 (1979).
 - ⁵⁶ C. Kittel and H. Kroemer, *Thermal Physics* (Freeman, San Francisco, 1980).
 - ⁵⁷ A. Zunger, in *Statics and Dynamics of Alloy Phase Transformations*, edited by P. E. A. Turchi and A. Gonis (Plenum New York, 1994), p. 361.
 - ⁵⁸ G. Burns, *Solid State Physics* (Academic Press, Orlando, Florida, 1985).
 - ⁵⁹ C. Bungaro, K. Rapcewicz, and J. Bernholc, *Phys. Rev. B* **61**, 6720 (2000).
 - ⁶⁰ A. F. Wright and J. S. Nelson, *Phys. Rev. B* **50**, 2159 (1994).
 - ⁶¹ H. Schulz and K. H. Thiemann, *Solid State Commun.* **23**, 815 (1977).
 - ⁶² K. Karch, J. M. Wagner, and F. Bechstedt, *Phys. Rev. B* **57**, 7043 (1998).

TABLE I: The SQS wurtzite (hcp) structure with 16 cations and 16 anions for $A_xB_{1-x}N$ alloys where A and B represent In and Ga cations, respectively, with $x = 1/4$ (or $x = 3/4$) and $x = 1/2$. The lattice vectors \mathbf{a}_1 , \mathbf{a}_2 , and \mathbf{a}_3 of the structures are linear combinations of the lattice vectors (i.e., \mathbf{a} , \mathbf{b} , and \mathbf{c}) of a hexagonal primitive cell. In Cartesian coordinates $\mathbf{a} = (a_0, 0, 0)$, $\mathbf{b} = (-a_0/2, a_0\sqrt{3}/2, 0)$ and $\mathbf{c} = (0, 0, c_0)$. The positions of the A cations are represented in the table as $A(\alpha, \beta, \gamma)$ corresponding to an A cation at the position $(\alpha\mathbf{a}_1 + \beta\mathbf{a}_2 + \gamma\mathbf{a}_3)/48$.

$x = 1/4$	$x = 1/2$
$\mathbf{a}_1 = 2\mathbf{a} - 2\mathbf{b} - 2\mathbf{c}$	$\mathbf{a}_1 = 2\mathbf{a} + 2\mathbf{b} - 2\mathbf{c}$
$\mathbf{a}_2 = \mathbf{a} + 2\mathbf{b}$	$\mathbf{a}_2 = 2\mathbf{a} + \mathbf{b} - \mathbf{c}$
$\mathbf{a}_3 = \mathbf{a} + \mathbf{b} + \mathbf{c}$	$\mathbf{a}_3 = 2\mathbf{a} - 2\mathbf{b} - 2\mathbf{c}$
A(39, 44, 6), A(18, 40, 36)	A(12, 16, 28), A(30, 8, 26)
A(24, 16, 0), A(27, 44, 30)	A(24, 16, 16), A(42, 8, 14)
B(0, 16, 0), B(3, 44, 30)	A(42, 8, 38), A(30, 8, 2)
B(6, 40, 12), B(9, 20, 42)	A(36, 16, 28), A(0, 16, 16)
B(42, 40, 36), B(45, 20, 18)	B(0, 16, 40), B(18, 8, 38)
B(12, 16, 24), B(15, 44, 6)	B(36, 16, 4), B(6, 8, 2)
B(36, 16, 24), B(21, 20, 18)	B(24, 16, 40), B(12, 16, 4)
B(30, 40, 12), B(33, 20, 42)	B(6, 8, 26), B(18, 8, 14)

TABLE II: The 16 cation SQS zinc-blende (fcc) structure for $A_xB_{1-x}N$ alloys. The lattice vectors \mathbf{a}_1 , \mathbf{a}_2 , and \mathbf{a}_3 are reported in terms of the lattice vectors of the primitive rhombohedral cell: $\mathbf{a} = a_0(0, 1/2, 1/2)$, $\mathbf{b} = a_0(1/2, 0, 1/2)$ and $\mathbf{c} = a_0(1/2, 1/2, 0)$. The positions of the A cations are represented in the table as $A(\alpha, \beta, \gamma)$ corresponding to an A cation at the position $(\alpha\mathbf{a}_1 + \beta\mathbf{a}_2 + \gamma\mathbf{a}_3)/16$.

$x = 1/4$	$x = 1/2$
$\mathbf{a}_1 = 2\mathbf{a} + \mathbf{b} - 2\mathbf{c}$	$\mathbf{a}_1 = 2\mathbf{a} - 2\mathbf{c}$
$\mathbf{a}_2 = \mathbf{a} + \mathbf{b} + 2\mathbf{c}$	$\mathbf{a}_2 = 2\mathbf{a} + 2\mathbf{b}$
$\mathbf{a}_3 = 2\mathbf{a} - \mathbf{b} + 2\mathbf{c}$	$\mathbf{a}_3 = 2\mathbf{a} - 2\mathbf{b}$
A(11, 12, 7), A(4, 0, 4)	A(8, 4, 4), A(0, 8, 8)
A(15, 12, 11), A(9, 4, 13)	A(8, 0, 8), A(0, 4, 12)
B(0, 0, 0), B(3, 12, 15)	A(8, 0, 0), A(0, 4, 4)
B(13, 4, 1), B(6, 8, 14)	A(8, 12, 4), A(0, 0, 8)
B(10, 8, 2), B(14, 8, 6)	B(0, 0, 0), B(8, 12, 12)
B(1, 4, 5), B(8, 0, 8)	B(0, 12, 4), B(8, 8, 0)
B(2, 8, 10), B(5, 4, 9)	B(0, 12, 12), B(8, 8, 8)
B(12, 0, 12), B(7, 12, 3)	B(0, 8, 0), B(8, 4, 12)

TABLE III: Lattice parameters of the wurtzite (WZ) and zinc-blende (ZB) structures for GaN and InN from the present study and other studies. u describes the displacement of the N (0001) planes from the Ga (0001) planes in units of c as described, in detail, in e.g., Ref. 58.

	$a(\text{\AA})$	$c(\text{\AA})$	u
GaN (WZ) Present calc.	3.145	5.121	0.377
Calc. ³⁸	3.196	5.206	0.376
Calc. ⁵⁹	3.20	5.22	0.376
Calc. ⁵¹	3.133	5.108	0.377
Calc. ⁶⁰	3.162	5.142	0.377
Expt. ⁶¹	3.190	5.189	0.377
InN (WZ) Present calc.	3.518	5.690	0.379
Calc. ³⁸	3.545	5.761	0.376
Calc. ⁵⁹	3.48	5.64	0.378
Calc. ⁴⁶	3.501	5.669	0.3784
Expt. ²	3.544	5.718	
GaN (ZB) Present calc.	4.443		
Calc. ⁶²	4.447		
InN (ZB) Present calc.	4.964		
Calc. ⁴⁶	4.932		

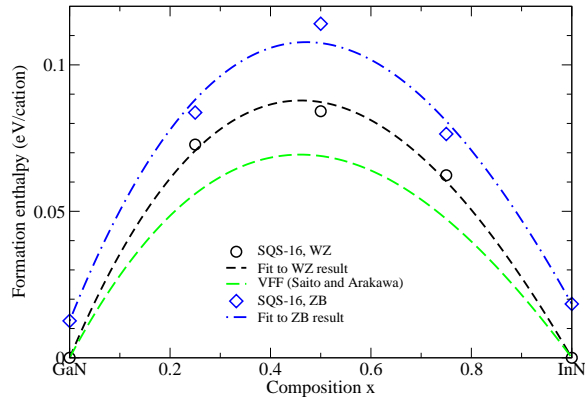


FIG. 1: (Color online) The formation enthalpy of wurtzite (WZ) and zinc-blende (ZB) $\text{In}_x\text{Ga}_{1-x}\text{N}$ as a function of composition x . The solid curve is a fit to the calculated values (open circles) with $(\alpha + \beta x)x(1 - x)$. The valence force field results of Saito and Arakawa¹⁶ are also included for comparison.

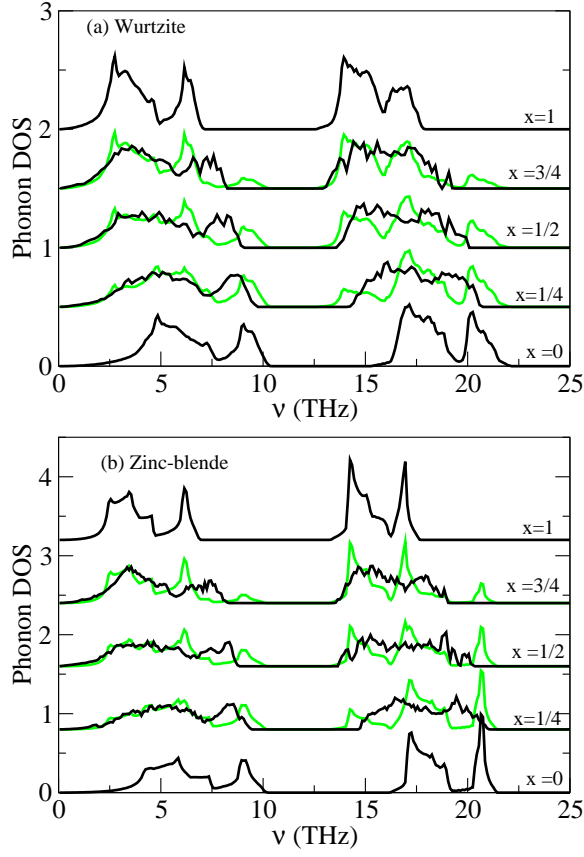


FIG. 2: (Color online) Phonon density of states (DOS) of (a) wurtzite and (b) zinc-blende $\text{In}_x\text{Ga}_{1-x}\text{N}$ correspond to $x = 0, 1/4, 1/2, 3/4$, and 1, which have been normalized according to $\int_0^\infty g(\nu)d\nu = 3$, where $\nu = \omega/2\pi$. An arbitrary shift is added to the curves for clarity. The black and grey curves refer to the solid solution system $g_{\text{In}_x\text{Ga}_{1-x}\text{N}}(\omega)$ and an average of the InN and GaN phases $g_{\text{av}}(\omega)$, respectively.

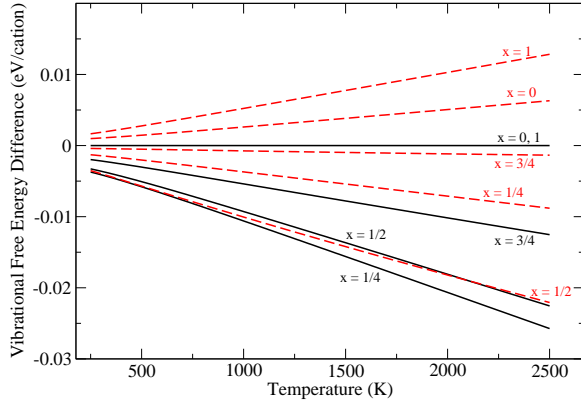


FIG. 3: (Color online) Vibrational free energy difference ΔG_v as a function of temperature, for the wurtzite (solid lines) and zinc-blende (dashed lines) structures.

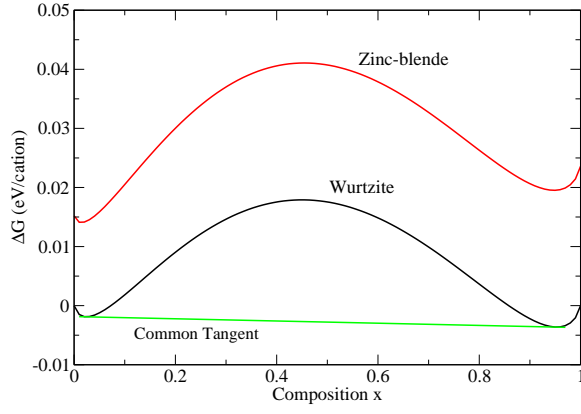


FIG. 4: (Color online) The common tangent intersects the wurtzite ΔG curve at $x_1 = 0.024$ and $x_2 = 0.95$, which gives the binodal curve in Fig. 5. Lattice vibrational effect has been taken into account. A representative case of $T = 1000$ K is used.

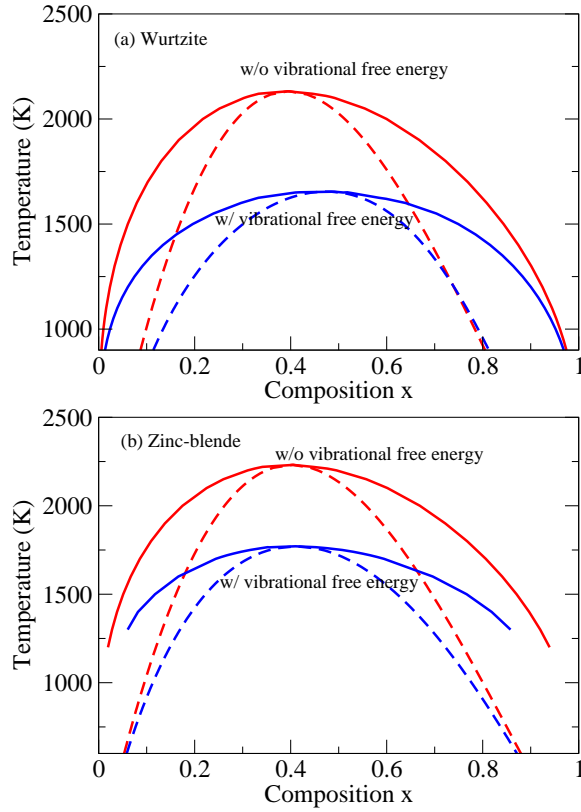


FIG. 5: (Color online) The pseudo-binary diagram (in temperature-cation concentration space) for (a) wurtzite and (b) zinc-blende $\text{In}_x\text{Ga}_{1-x}\text{N}$ with and without the inclusion of lattice vibration effects. The solid lines correspond to the equilibrium binodal curves and the dashed lines represent the spinodal curves.

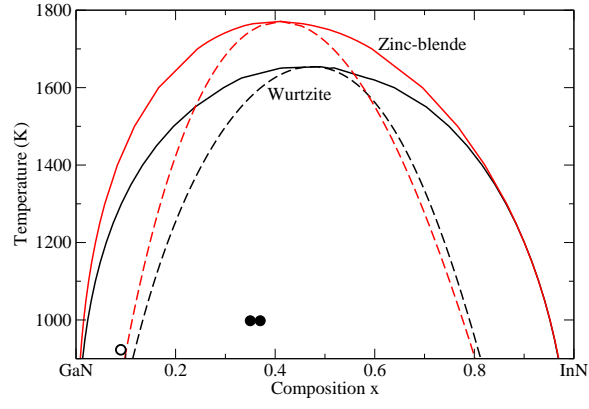


FIG. 6: (Color online) A comparison of the pseudo-binary diagrams of zinc-blende and wurtzite $\text{In}_x\text{Ga}_{1-x}\text{N}$ (including the effects of lattice vibrations). The solid lines correspond to the equilibrium binodal curves and the dashed lines represent the spinodal curves. The points represented by the filled and open circles represent the experimental data⁴ for which phase separation was and was not observed, respectively.